

Pair Production by Photons: Exact Calculation for Unscreened Atomic Field

Ingjald Øverbø,* Kjell J. Mork, and Haakon A. Olsen

Institute of Physics, University of Trondheim, NLHT, Trondheim, Norway

(Received 3 October 1972)

Exact relativistic Coulomb wave functions, in the form of partial-wave expansions, are used to obtain analytic formulas for the differential cross sections and energy spectrum for electron-positron pair production by photons. Radiative corrections, which are believed to be small (of the order of 1%), are neglected. The errors introduced by the finite nuclear size and recoil effects are quite negligible for the energy region considered here. Apart from these approximations, the present formulas give the exact cross sections for the unscreened atomic field. Numerical results are obtained for positron energy spectra for a large number of photon energies and atomic numbers in the ranges $2m_e c^2 < k \leq 10m_e c^2$ and $1 \leq Z \leq 100$. Total cross sections are obtained by numerical integration of the spectra. A representative choice of spectra is given. The approximately 500 total cross sections calculated are given in tables and diagrams. By one- or two-way interpolation in these data the total cross section for any photon energy and nuclear charge within the given limits may be obtained with an accuracy of 1% or better. For heavy elements large Coulomb corrections to the Bethe-Heitler Born-approximation results are found. The positron energy spectra obtained are asymmetric, favoring positrons of high energy. The total cross section σ is smaller than the Bethe-Heitler total cross section σ_B for photon energies very close to the threshold (owing to the repulsion of the positron), while σ is generally larger than σ_B in the energy region $2.2m_e c^2 \lesssim k \lesssim 10m_e c^2$.

I. INTRODUCTION

The problem of obtaining relativistic Coulomb corrections to the Born-approximation cross-section formulas for processes like pair production, bremsstrahlung, and the photoelectric effect is almost as old as the Born-approximation calculations themselves.

Jaeger and Hulme¹ made calculations on internal conversion using relativistic Coulomb wave functions, as partial-wave expansions, as early as 1935. They also obtained a few results for pair production,² finding that the exact cross section was a factor 2 larger than the Born-approximation result for $Z=82$ and a photon energy $k=3m_e c^2$.

This deviation was not surprising. The Born approximation should be valid only for $\alpha ZE/p \ll 1$, suggesting that for heavy elements the Bethe-Heitler formula is a crude approximation even for high energies, and of course worse for low energies, as E/p increases. When the first measurements of the high-energy pair-production total cross section were made around 1950, it was therefore a surprise that the results were only about 10% below the Bethe-Heitler value for lead. These results were confirmed by Davies, Bethe, and Maximon,³ who used the approximate Furry-Sommerfeld-Maue wave function to calculate the Coulomb correction, in a high-energy approximation.

For photon energies below 20–30 MeV the Davies-Bethe-Maximon high-energy approximation breaks down. Besides, the Furry-Sommerfeld-Maue wave function itself is not good for large Z

and small energies.⁴ In order to obtain Coulomb corrections for low energies it was therefore necessary to turn to the exact Coulomb partial-wave method again. This method has, although it is complicated, become much more powerful through the development of the modern electronic computer.

The main difficulty is the evaluation of the radial parts of the matrix elements. The methods used to evaluate these may be divided into two categories, of which the first is to integrate the radial integrals analytically. The integrals may then be expressed in terms of generalized hypergeometric functions, which are more or less difficult to evaluate numerically. This may be called the analytic method. The other method is to perform the radial integrals numerically, using numerical solutions of the radial wave equations. While the analytic method applies only to Coulomb wave functions, this numerical method has the advantage of being applicable to screened potentials. On the other hand its usefulness seems to be limited rather strongly by the fact that it requires much more computer time than the analytic method.

The early calculations^{1,2} were based on the analytic method. So also was the work by Hultberg *et al.* on the K -shell photoelectric cross section in 1962,⁵ calculations by Rozics and Johnson on bremsstrahlung,⁶ and by Alling and Johnson on the photoelectric effect.⁷ Matese and Johnson used a modified analytic approach in an attempt to calculate also screening corrections for the photoelectric effect.⁸

A numerical method was applied by Pratt *et al.*

for calculations on the photoelectric effect (unscreened Coulomb potential).⁹ Similar calculations with screened-potential models were performed by Hall and Sullivan,¹⁰ Rakavy and Ron,¹¹ Schmickley and Pratt,¹² and Brysk and Zerby.¹³ Brysk, Zerby, and Penny used a numerical method for calculations on bremsstrahlung (with a screened potential).¹⁴ Similar calculations were carried out by Tseng and Pratt for bremsstrahlung and pair production.¹⁵

For the photoelectric effect the numerical method has been used to obtain rather extensive numerical results. In bremsstrahlung and pair production, however, we have two free fermions, and the number of matrix elements becomes so large that the numerical method is of limited use.¹⁴⁻¹⁵

In the present work we use an analytic method to obtain extensive numerical results for the Coulomb correction to the pair-production energy spectrum and total cross section for photon energies $k \leq 10m_e c^2$.^{16,17} Sections II and III contain a short discussion of the Coulomb wave functions and the matrix element. The angular and radial parts of the latter are treated in Sec. IV. In Sec. V we integrate the differential cross section and obtain a formula for the positron energy spectrum.

Almost all the existing experimental data on low-energy pair production concern the total cross section. A few measurements of differential cross sections have been reported, but mostly for energies far above the present range. In this work we therefore confine ourselves to calculate energy spectra, from which the total cross sections are obtained by numerical integration.

The evaluation of numerical results requires rather complicated computer programs, and for some of the results the procedure of calculation is very delicate and time consuming.¹⁶ In Sec. VI we therefore give a detailed description of the results, in the hope of making them as easily accessible as possible. We have calculated the energy spectrum and the total cross section for about 500 different combinations of photon energy and atomic number in the ranges $2m_e c^2 < k \leq 10m_e c^2$ (i.e., $1.022 < k < 5.11$ MeV) and $1 \leq Z \leq 100$. A representative choice of spectra is given in diagrams. The emphasis is on the total cross section, which is presented in tables and diagrams. From these it should be possible to find the total cross section by interpolation for any photon energy and atomic number within the given limits, with an accuracy of the order 1%.

The calculations are based on a simple vertex diagram in the Furry picture, that is, a photon line connected to two fermion lines which correspond to Coulomb wave functions. Thus we ne-

glect radiative corrections. For high-energy pair production the radiative corrections to the total cross section amount to about 1%.¹⁸ For the intermediate energy region no results have been given, but it does not seem unreasonable to assume that the correction is of the same relative order of magnitude for the whole relativistic domain. For nonrelativistic energies the radiative corrections are negligible.¹⁹

Our use of Coulomb wave functions implies that we regard the atomic nucleus as an infinitely heavy point charge. However, the errors introduced by the neglect of the finite nuclear size and recoil effects are quite negligible for the present energy region. For comparison with experiments one has to take into account the screening effect from the atomic electrons. For the major part of the energy region considered here (say $3m_e c^2 \leq k \leq 10m_e c^2$) the screening effect gives small corrections, of the order of a few percent. For the threshold region $2m_e c^2 < k \leq 3m_e c^2$, however, the screening is important, as argued by Øverbø¹⁶ and as shown by the calculations of Tseng and Pratt.¹⁵ As previously mentioned, the analytic method does not allow us to treat screened potentials exactly. However, it is possible to use an approximate method to obtain very good screening corrections to our exact Coulomb results. This we plan to do in a subsequent paper, where we shall also compare with experiments.

II. WAVE FUNCTIONS

The spherical-wave solution of the Dirac equation with a central potential $V = V(r)$ may be written (we use units $\hbar = c = m_e = 1$)

$$\phi_{\kappa\mu}(E, V, \vec{r}) = \begin{pmatrix} \frac{E+1}{2E} \left(g_{\kappa}(V, r) \chi_{\kappa\mu}(\hat{r}) \right) \\ i f_{\kappa}(V, r) \chi_{-\kappa\mu}(\hat{r}) \end{pmatrix}, \quad (2.1)$$

where

$$\chi_{\kappa\mu}(\hat{r}) \equiv \chi_{j\mu l}(\hat{r}) = \sum_{\nu=\pm\frac{1}{2}} \langle j\mu | l \mu - \nu \frac{1}{2} \nu \rangle Y_l^{\mu-\nu}(\hat{r}) \chi^{\nu}; \quad (2.2)$$

$\langle j\mu | l m \frac{1}{2} \nu \rangle$ is a Clebsch-Gordan coefficient, Y_l^m is the spherical harmonic, and $\chi^{\nu}(\nu = \pm \frac{1}{2})$ is the Pauli spinor.²⁰ Our notation is further explained by the eigenvalue equations

$$\left\{ \begin{array}{l} -i \vec{\alpha} \cdot \nabla + \beta + V(r) - E \\ \beta (\vec{\sigma} \cdot \vec{L} + 1) + \kappa \\ J_z - \mu \end{array} \right\} \phi_{\kappa\mu}(E, V, \vec{r}) = 0, \quad (2.3)$$

$$\left\{ \begin{array}{l} \vec{\sigma} \cdot \vec{L} + 1 + \kappa \\ J_z - \mu \\ L^2 - l(l+1) \\ J^2 - j(j+1) \end{array} \right\} \chi_{\kappa\mu}(\hat{r}) = 0, \quad (2.4)$$

where

$$\vec{\alpha} = \begin{pmatrix} 0 & \vec{\sigma} \\ \vec{\sigma} & 0 \end{pmatrix} \quad \text{and} \quad \beta = \begin{pmatrix} 1 & 0 \\ 0 & -1 \end{pmatrix}$$

are the Dirac matrices, $\vec{\sigma}$ is the Pauli spin operator, and \vec{L} and $\vec{J} = \vec{L} + \frac{1}{2}\vec{\sigma}$ are the orbital and total angular momentum operators. The quantum numbers κ and μ assume the values

$$\kappa = \pm 1, \pm 2, \dots, \quad \mu = \pm \frac{1}{2}, \pm \frac{3}{2}, \dots, \quad \pm(|\kappa| - \frac{1}{2}). \quad (2.5)$$

The following relations are frequently used:

$$\begin{aligned} j &\equiv j_\kappa = |\kappa| - \frac{1}{2}, \quad l \equiv l_\kappa = j + \frac{1}{2}\kappa/|\kappa|, \\ l_{-\kappa} &\equiv l'_\kappa = j - \frac{1}{2}\kappa/|\kappa|. \end{aligned} \quad (2.6)$$

In the Coulomb case, with $V = -\alpha Z/r$, the radial equations

$$\frac{df}{dr} + \frac{(1-\kappa)f}{r} + (E - V - 1)g = 0, \quad (2.7)$$

$$\frac{dg}{dr} + \frac{(1+\kappa)g}{r} - (E - V + 1)f = 0$$

have a well-known²¹⁻²⁵ analytic solution, which we write in the form

$$\begin{cases} g_\kappa(r) \\ f_\kappa(r) \end{cases} = \begin{cases} 1 \\ i\hat{p}/(E+1) \end{cases} \left\{ \frac{(2\hat{p}r)^{\gamma-1} e^{\pi y/2} |\Gamma(\gamma + iy)|}{\Gamma(2\gamma + 1)} (H_\pm H^*) \right\}, \quad (2.8)$$

where

$$H = (\gamma + iy) e^{i\eta - i\hat{p}r} {}_1F_1(\gamma + 1 + iy; 2\gamma + 1; 2i\hat{p}r)$$

and

$$e^{i\eta} = S \frac{(\kappa - \gamma)\hat{p} + i\alpha Z(E - 1)}{[2(E - 1)(E\kappa - \gamma)(\kappa - \gamma)]^{1/2}}, \quad (2.9)$$

where the sign S may be chosen arbitrarily. Asymptotically

$$\begin{aligned} g_\kappa(r) &\underset{r \rightarrow \infty}{\sim} (\hat{p}r)^{-1} \sin(\hat{p}r - \frac{1}{2}\pi l + \delta_\kappa), \\ f_\kappa(r) &\underset{r \rightarrow \infty}{\sim} \hat{p}(E+1)^{-1} (\hat{p}r)^{-1} \cos(\hat{p}r - \frac{1}{2}\pi l + \delta_\kappa), \end{aligned} \quad (2.10)$$

where

$$\delta_\kappa = \eta - \arg \Gamma(\gamma + iy) + y \ln 2\hat{p}r - \frac{1}{2}\pi\gamma + \frac{1}{2}\pi(l + 1). \quad (2.11)$$

In the preceding equations

$$\begin{aligned} \hat{p} &= (E^2 - 1)^{1/2}, \\ y &= \alpha ZE/\hat{p}, \\ \gamma &= [\kappa^2 - (\alpha Z)^2]^{1/2}, \end{aligned} \quad (2.12)$$

and Γ and ${}_1F_1$ represent the gamma and confluent hypergeometric functions.

The formulas given above are valid for all $|E| > 1$, which is convenient for the handling of positron wave functions, as discussed in what follows.

In (2.8) the radial functions g and f appear essentially as the real and imaginary parts of a complex-valued Whittaker function. We notice that g and f may also be expressed in terms of real-valued functions of the type $e^{-i\hat{p}r} {}_1F_1(\gamma + iy; 2\gamma; 2i\hat{p}r)$.^{26,27}

The spherical wave functions $\phi_{\kappa\mu}(E, Z, \vec{r})$ constitute a complete set of states for the Coulomb field, in the sense that any state of given energy, satisfying the Dirac equation with $V = -\alpha Z/r$, may be expanded in terms of the spherical waves of the same energy. Fermions whose angular distributions are not observed may therefore be represented directly by the spherical wave functions.

For the case where the angular distribution of a fermion is observed, it is well known that this particle must be represented by a solution of the Dirac equation which behaves asymptotically *essentially* like a plane wave plus diverging or converging spherical waves, depending on whether the fermion is in an initial or final state.²⁸ The well-known solutions for the Coulomb case are^{23,29}

$$\begin{aligned} \Phi_\pm(\hat{p}, E, \vec{\xi}, Z) &= 4\pi \sum_{\kappa\mu} i^l e^{\pm i\delta'_\kappa} \\ &\times [\chi_{\kappa\mu}^\pm(\hat{p}) v(\vec{\xi})] \phi_{\kappa\mu}(E, Z, \vec{r}), \end{aligned} \quad (2.13)$$

respectively, where

$$\delta'_\kappa \equiv \delta_\kappa - y \ln 2\hat{p}r = \eta - \arg \Gamma(\gamma + iy) - \frac{1}{2}\pi\gamma + \frac{1}{2}\pi(l + 1),$$

and the unit vector $\vec{\xi} = v^\dagger(\vec{r}) \vec{\sigma} v(\vec{r})$ gives the spin direction in the rest system of the electron.³⁰

Asymptotically²³

$$\Phi_\pm \underset{r \rightarrow \infty}{\sim} a e^{i[\vec{p} \cdot \vec{r} \mp y \ln(\hat{p}r \mp \vec{p} \cdot \vec{r})]} + (b^\pm(\hat{r})/r) e^{\pm i(\hat{p}r \mp y \ln 2\hat{p}r)},$$

where

$$a = \left(\frac{E+1}{2E} \right)^{1/2} \left(\vec{\sigma} \cdot \vec{p} / (E+1) \right) v(\vec{\xi});$$

i.e., the wave functions (2.13) are normalized to unit volume.

Positron wave functions are obtained by changing the sign of the fermion charge in the Dirac equation. For the Coulomb potential this is equivalent to the substitution $Z \rightarrow -Z$, which means that a positron wave function Φ^c may be obtained from an electron wave function Φ by the formula

$$\Phi^c(\hat{p}, E, \vec{\xi}, Z) = \Phi(\hat{p}, E, \vec{\xi}, -Z). \quad (2.14)$$

It is easily shown from the Dirac equation that

$$\Phi_\pm(\hat{p}, E, \vec{\xi}, Z) = S \gamma_2 \Phi_\pm^*(-\hat{p}, -E, \vec{\xi}', Z), \quad (2.15)$$

where the asterisk means complex conjugation, S is an appropriate sign which is unimportant, and $\vec{\xi}'$ and $\vec{\xi}$ are related by the well-known formula

$$\vec{\xi}' = \vec{\xi} - 2\hat{p}(\hat{p} \cdot \vec{\xi}), \quad (2.16)$$

corresponding to

$$v(\vec{\xi}') = i\vec{\sigma} \cdot \hat{p}\sigma_y v^*(\vec{\xi}).$$

III. MATRIX ELEMENTS

It is a well-known fact that the matrix element for pair production is related to that for bremsstrahlung by a very simple rule of substitution. The matrix element for bremsstrahlung, corresponding to the simple vertex diagram mentioned in the Introduction, may be written

$$\mathfrak{M}_B = \int \Phi_-^\dagger(\hat{p}_2, E_2, \vec{\xi}_2, Z) \vec{\alpha} \cdot \vec{e}^* \times \Phi_+(\hat{p}_1, E_1, \vec{\xi}_1, Z) e^{-i\vec{k} \cdot \vec{r}} d^3x, \quad (3.1)$$

where Φ_\pm are given by (2.13), $\vec{\alpha} = \begin{pmatrix} 0 & \vec{\sigma} \\ \vec{\sigma} & 0 \end{pmatrix}$, and \vec{e} is the polarization vector and \vec{k} the momentum of the emitted photon. The unit vectors \hat{p}_1 and \hat{p}_2 give the directions of motion, and E_1 and E_2 are the energies of the initial and final electrons, respectively.

We obtain the pair-production matrix element by replacing $\vec{e}^* e^{-i\vec{k} \cdot \vec{r}}$ by $\vec{e} e^{i\vec{k} \cdot \vec{r}}$, corresponding to annihilation instead of creation of a photon, and by replacing the wave function Φ_+ of the initial electron by $\gamma_2 \Phi_-^{c*}$, where Φ^c is a positron wave function as defined by (2.14). According to (2.15) the expression $\gamma_2 \Phi_-^{c*}(\hat{p}_+, E_+, \vec{\xi}_+, Z)$ is identical to the wave function $\Phi_+(-\hat{p}_+, -E_+, \vec{\xi}_+, Z)$, with the relation (2.16) between $\vec{\xi}$ and $\vec{\xi}_+$. (The index + denotes the positron quantities.) This means that the final-state positron is replaced by an initial-state negative-energy electron, moving in the opposite direction.

In the following we shall evaluate a matrix element of the form

$$\mathfrak{M} = \int \Phi_-^\dagger(\hat{p}_2, E_2, \vec{\xi}_2, Z) \vec{\alpha} \cdot \vec{e} \times \Phi_+(\hat{p}_1, E_1, \vec{\xi}_1, Z) e^{i\vec{k} \cdot \vec{r}} d^3x. \quad (3.2)$$

From the resulting formula one may then obtain \mathfrak{M}_B by the substitutions

$$\begin{aligned} \vec{e} &\rightarrow \vec{e}^*, \\ \vec{k} &\rightarrow -\vec{k}, \end{aligned} \quad (3.3)$$

while the pair-production matrix element \mathfrak{M}_P will be obtained from \mathfrak{M} by the substitutions

$$\begin{aligned} \hat{p}_1 &\rightarrow -\hat{p}_+, \\ E_1 &\rightarrow -E_+, \\ \vec{\xi}_1 &\rightarrow \vec{\xi}_+ - 2\hat{p}_+(\hat{p}_+ \cdot \vec{\xi}_+). \end{aligned} \quad (3.4)$$

Insertion of (2.13) into (3.2) gives

$$\mathfrak{M} = (4\pi)^2 \sum_{\kappa_1 \mu_1 \kappa_2 \mu_2} \{ i^{l_1 - l_2} e^{i(\delta_2' + \delta_1')} [\chi_{\kappa_2 \mu_2}^\dagger(\hat{p}_2) v(\vec{\xi}_2)]^* \times [\chi_{\kappa_1 \mu_1}^\dagger(\hat{p}_1) v(\vec{\xi}_1)] \mathfrak{M}_{\kappa_2 \mu_2 \kappa_1 \mu_1} \}, \quad (3.5)$$

where l_1 and δ_1' are shorthand for l_{κ_1} and δ'_{κ_1} [cf. Eqs. (2.6) and (2.13)], and

$$\mathfrak{M}_{\kappa_2 \mu_2 \kappa_1 \mu_1} = \int \phi_{\kappa_2 \mu_2}^\dagger(E_2, Z, \vec{r}) \begin{pmatrix} 0 & 1 \\ 1 & 0 \end{pmatrix} \vec{\sigma} \cdot \vec{e} \times \phi_{\kappa_1 \mu_1}(E_1, Z, \vec{r}) e^{i\vec{k} \cdot \vec{r}} d^3x \quad (3.6)$$

is a matrix element between spherical wave functions given by (2.1). We choose our coordinate system with $\hat{z} = \hat{k}$ and may then substitute

$$e^{i\vec{k} \cdot \vec{r}} = e^{ikz} = 4\pi \sum_{L=0}^{\infty} i^L j_L(kr) [(2L+1)/4\pi]^{1/2} Y_L^0(\hat{r}),$$

where j_L is the spherical Bessel function. Defining the "plus" and "minus" components of a vector \vec{a} by

$$a_\pm = 2^{-1/2}(a_x \pm ia_y), \quad (3.7)$$

we may write

$$\vec{\sigma} \cdot \vec{e} = \sigma_+ e_- + \sigma_- e_+.$$

(We work in the Coulomb gauge, with $\vec{e} \cdot \hat{k} = \vec{e} \cdot \hat{z} = 0$.) Substituting into (3.6) we arrive at the following expression:

$$\begin{aligned} \mathfrak{M}_{\kappa_2 \mu_2 \kappa_1 \mu_1} &= \frac{1}{2k} [2\hat{p}_2 E_2 \hat{p}_1 |E_1|]^{-1/2} \\ &\times \sum_{\epsilon = \pm} e_{-\epsilon} \delta_{M, \mu_2 - \epsilon/2} \delta_{M, \mu_1 + \epsilon/2} A_{\kappa_2 \kappa_1 M}^\epsilon, \end{aligned} \quad (3.8)$$

where δ_{ik} is the Kronecker- δ symbol and

$$\begin{aligned} A_{\kappa_2 \kappa_1 M}^\epsilon &= \begin{cases} -\kappa_2/|\kappa_2| & \text{when } \epsilon = + \\ \kappa_1/|\kappa_1| & \text{when } \epsilon = - \end{cases} \sum_{L=0}^{\infty} i^{L+1} \left\{ \left[\frac{(\kappa_2 - \epsilon M)(\kappa_1 - \epsilon M)}{(2\kappa_2 + 1)(2\kappa_1 - 1)} \right]^{1/2} V(l_2 L l_1' M) R_{\kappa_2 L \kappa_1}^+ \right. \\ &\quad \left. + \left[\frac{(\kappa_2 + \epsilon M)(\kappa_1 + \epsilon M)}{(2\kappa_2 - 1)(2\kappa_1 + 1)} \right]^{1/2} V(l_2' L l_1 M) R_{\kappa_2 L \kappa_1}^- \right\}, \end{aligned} \quad (3.9)$$

where l_1' is shorthand for l'_{κ_1} , defined by (2.6). The angular integrals

$$V(l_2 L l_1 M) \equiv [4\pi(2L+1)]^{1/2} \int Y_L^0 Y_{l_2}^M * Y_{l_1}^M d\Omega \quad (3.10)$$

and the radial integrals

$$R_{\kappa_2 L \kappa_1}^\pm \equiv 2k [p_2(E_2 + 1) p_1 |E_1 + 1|]^{1/2} \times \int_0^\infty r^2 j_L(kr) \left\{ \begin{matrix} g_{\kappa_2}(E_2) f_{\kappa_1}(E_1) \\ f_{\kappa_2}(E_2) g_{\kappa_1}(E_1) \end{matrix} \right\} dr \quad (3.11)$$

are treated in Sec. IV. [The factors in front of (3.8) and (3.11) are a choice of convenience.]

IV. ANGULAR AND RADIAL INTEGRALS

The angular integrals (3.10) are given by standard formulas as products of two Clebsch-Gordan coefficients,²⁰

$$V(l_2 L l_1 M) = (2L + 1) \left(\frac{2l_2 + 1}{2l_1 + 1} \right)^{1/2} \times \langle l_1 0 | L 0 l_2 0 \rangle \langle l_1 M | L 0 l_2 M \rangle. \quad (4.1)$$

If $2t \equiv l_2 + L + l_1$ is an odd integer,

$$V(l_2 L l_1 M) = (-)^{t_1 + t} (2L + 1) [(2l_2 + 1)(2l_1 + 1)]^{1/2} \frac{(l_2 + L - l_1)! (l_2 + l_1 - L)! (L + l_1 - l_2)!}{(L + l_1 + l_2 + 1)!} \times \frac{t!}{(t - l_2)! (t - l_1)! (t - L)!} \sum_K \frac{(-)^K L! [(l_2 + M)! (l_2 - M)! (l_1 + M)! (l_1 - M)!]^{1/2}}{K! (l_2 + L - l_1 - K)! (l_2 - M - K)! (L - K)! (l_1 - L + M + K)! (l_1 - l_2 + K)!}, \quad (4.5)$$

where the summation index K assumes all integer values for which all the factorial arguments are nonzero.

As already mentioned in Sec. I, the radial integrals (3.11) constitute the main problem in our calculations. Analytic expressions for R^\pm may be obtained in two ways: (i) by making use of the fact that the spherical Bessel function is a special case of the Whittaker function,

$$j_L(kr) = \frac{\pi^{1/2}}{2\Gamma(L + \frac{3}{2})} \left(\frac{kr}{2} \right)^L e^{-ikr} {}_1F_1(L + 1; 2L + 2; 2ikr); \quad (4.6)$$

(ii) by using the finite-series expansion

$$j_L(kr) = \sum_{n=0}^L \frac{(L+n)!}{n!(L-n)!} \left(\frac{1}{2kr} \right)^{n+1} (i^{L+1-n} e^{-ikr} + c.c.), \quad (4.7)$$

where c.c. means complex conjugate. In the present work we use (4.7), which gives R^\pm expressed in terms of Appell functions F_2 , as shown in what follows. An analogous derivation based on (4.6) would lead to expressions in terms of Lauricella functions F_A of three variables. Both of these functions are generalizations of the ordinary (Gauss) hypergeometric function ${}_2F_1$.^{32,33}

Before proceeding to evaluate the integral we notice that the integrand of (3.11) behaves for small r essentially as

$$V(l_2 L l_1 M) = 0. \quad (4.2)$$

This is easily seen from (3.10), since Y_l^m has the parity $(-)^l$. One may also easily verify that

$$V(l_2 L l_1 M) = V(l_2 L l_1 - M) = V(l_1 L l_2 M); \quad (4.3)$$

i.e., the angular integral V is an even function of M and it is symmetrical with respect to l_2 and l_1 . The angular integrals limit the summations over L in (3.9) and over M (i.e., over μ_2 and μ_1) in (3.5), since $V(l_2 L l_1 M)$ is only different from zero when

$$|l_2 - l_1| \leq L \leq l_2 + l_1 \quad \text{and} \quad |M| \leq \min(l_2, l_1). \quad (4.4)$$

For $t \equiv \frac{1}{2}(l_2 + L + l_1) = \text{integer}$, the explicit formula³¹ is

$$r^{\gamma_2 + \gamma_1 + L},$$

and for large r essentially as r^{-1} times a product of sines and cosines. Thus the integral converges (but not absolutely) for large r . According to Abel's test³⁴ the integral $R(\epsilon)$, defined by (3.11) with an additional factor $e^{-\epsilon r}$ in the integrand, is then uniformly convergent (in ϵ) for $\epsilon \geq 0$. Hence the integral $R(\epsilon)$ is continuous for $\epsilon \geq 0$, and we are allowed to take the limit $\epsilon \rightarrow 0$ (the Abelian limit) after the integration. The convenience of this operation becomes clear in the following.

Insertion of (2.8) and (4.7) into (3.11) now gives integrals of the form

$$E_n^\pm(\epsilon) = -(i/2) \int_0^\infty r^{\gamma_1 + \gamma_2 - n - 1} e^{-\epsilon r} (J + J^*) \times (H_1 \mp H_1^*)(H_2 \pm H_2^*) dr,$$

where H is given by (2.8) and $J \equiv i^{L+1-n} e^{-ikr}$. Since $(H_1 \mp H_1^*)(H_2 \pm H_2^*)$ is pure imaginary, we may write

$$E_n^\pm(\epsilon) = \text{Im} \left\{ \int_0^\infty r^{\gamma_1 + \gamma_2 - n - 1} e^{-\epsilon r} \times J(H_1 \mp H_1^*)(H_2 \pm H_2^*) dr \right\}. \quad (4.8)$$

It follows from (4.4) that the index n , which is introduced by (4.7), is limited by

$$0 \leq n \leq |\kappa_1| + |\kappa_2|.$$

All the integrals (4.8) are therefore convergent for large values of r . For small r the integrals behave like

$$\int_0 r^{\gamma_1 + \gamma_2 - n - 1} dr;$$

i.e., they all converge except for the case $n = n_{\max} = L_{\max} = |\kappa_1| + |\kappa_2|$ (for $Z \geq 119$ the integral is also divergent for $n = L_{\max} - 1$). We avoid this divergence problem, which is due to the expansion (4.7), by considering, instead of (4.8), the integrals

$$E_n^\pm(\epsilon, \xi) \equiv \text{Im} \left\{ \int_0^\infty r^{\gamma_1 + \gamma_2 - n - 1 + \xi} e^{-\epsilon r} \times J(H_1 \mp H_1^*)(H_2 \pm H_2^*) dr \right\}, \quad (4.9)$$

where $\epsilon > 0$ and

$$\xi > \xi_0 \equiv \max(|\kappa_1| + |\kappa_2| - \gamma_1 - \gamma_2) = 2 - 2[1 - (\alpha Z)^2]^{1/2}. \quad (4.10)$$

With this condition the integrals in (4.9) are convergent for all $Z \leq 137$ and may be evaluated analytically. The resulting formula for $R_{\kappa_2 \kappa_1}^\pm(\epsilon, \xi)$ may be continued analytically to $\xi = 0$, as shown in the following.

The combination JH_1H_2 in (4.9) gives an integral

$$I(\epsilon, \xi) \equiv \int_0^\infty r^{a-1+\xi} e^{-r[\epsilon + (t_1+t_2+2ik)/2]} \times {}_1F_1(b_1; c_1; t_1 r) {}_1F_1(b_2; c_2; t_2 r) dr, \quad (4.11)$$

where

$$\begin{aligned} a &= \gamma_1 + \gamma_2 - n, & t_1 &= 2i\dot{p}_1, & b_1 &= \gamma_1 + 1 + iy_1, \\ c_1 &= 2\gamma_1 + 1, & l &= 1, 2. \end{aligned} \quad (4.12)$$

$$\begin{aligned} I(\epsilon, \xi) &= \frac{\Gamma(a+\xi)}{[\epsilon + \frac{1}{2}(t_1+t_2+2ik)]^{a+\xi}} G_1 G_2 \int_0^1 \int_0^1 \frac{u_1^{b_1-1} (1-u_1)^{c_1-b_1-1} u_2^{b_2-1} (1-u_2)^{c_2-b_2-1}}{(1-u_1 z_1 - u_2 z_2)^{a+\xi}} \\ &\equiv \frac{\Gamma(a+\xi)}{[\epsilon + \frac{1}{2}(t_1+t_2+2ik)]^{a+\xi}} F_2(a+\xi; b_1, b_2; c_1, c_2; z_1, z_2), \end{aligned} \quad (4.14)$$

since $G_1 G_2$ times the double integral is identical to a standard integral representation for the Appell function F_2 .^{32,33} (The double integral exists, because the complex quantity $\zeta \equiv 1 - u_1 z_1 - u_2 z_2$ is never outside a parallelogram in the complex ζ plane with one corner at $\zeta = 1$ and the other three in the lower half-plane, provided that $\epsilon > 0$.) We notice that the Γ function in (4.14) has simple poles for $\xi = \xi_0, \xi_0 - 1, \xi_0 - 2$, etc., where $0 < \xi_0 < 2$, according to (4.10). Thus one or two of the poles are on the positive real ξ axis. [These singularities are, however, spurious, since the total radial integral (3.11), with the additional

The other three combinations in (4.9) also lead to integrals of the form (4.11), when we use the Kummer transformation on the terms H_1^* and H_2^* . Using the standard integral representation

$$\begin{aligned} {}_1F_1(b; c; tr) &= \frac{\Gamma(c)}{\Gamma(b)\Gamma(c-b)} \\ &\times \int_0^1 e^{tru} u^{b-1} (1-u)^{c-b-1} du, \end{aligned}$$

we now get

$$\begin{aligned} I(\epsilon, \xi) &= \int_0^\infty r^{a-1+\xi} e^{-rU} G_1 G_2 \\ &\times \int_0^1 \int_0^1 u_1^{b_1-1} (1-u_1)^{c_1-b_1-1} \\ &\times u_2^{b_2-1} (1-u_2)^{c_2-b_2-1} du_1 du_2 dr, \end{aligned}$$

where

$$U \equiv \epsilon + \frac{1}{2}(t_1+t_2+2ik) - t_1 u_1 - t_2 u_2$$

and

$$G_l = \frac{\Gamma(c_l)}{\Gamma(b_l)\Gamma(c_l-b_l)}, \quad l=1, 2.$$

With $\epsilon > 0$ we can perform the integration over r first, obtaining

$$\int_0^\infty r^{a-1+\xi} e^{-rU} dr = \Gamma(a+\xi) U^{-a-\xi}, \quad (4.13)$$

with

$$|\arg U| < \frac{1}{2}\pi.$$

Writing

$$z_l = \frac{t_l}{\epsilon + \frac{1}{2}(t_1+t_2+2ik)} = \frac{2\dot{p}_l}{\dot{p}_1 + \dot{p}_2 + k - i\epsilon}, \quad l=1, 2$$

we then have

factors $r^\xi e^{-\epsilon r}$ in the integrand, is regular for $\xi \geq 0$.] Except for the poles, the right-hand side of (4.14) is analytic in the ξ plane. Hence we can take the limit $\xi \rightarrow 0$ by analytic continuation, and the only problem left is to find

$$\tilde{F}_2(b_1, b_2) \equiv \lim_{\epsilon \rightarrow 0} F_2(a; b_1, b_2; c_1, c_2; z_1, z_2). \quad (4.15)$$

For the case of pair production we can take the limit $\epsilon \rightarrow 0$ at once, because for this process we have

$$k = E_+ + E_2 > \dot{p}_+ + \dot{p}_2 = \dot{p}_1 + \dot{p}_2.$$

Therefore

$$\lim_{\epsilon \rightarrow 0} (|z_1| + |z_2|) = \frac{2(p_1 + p_2)}{k + p_1 + p_2} < 1, \quad (4.16)$$

and the factor $(1 - u_1 z_1 - u_2 z_2)^{-a}$ appearing in (4.14) can be expanded in a double binomial series, lead-

ing to the fundamental double-series representation for the Appell function F_2 .^{32,33} Including all the factors from (2.8), (3.11), and (4.7) we may then write our radial integrals in the following way:

$$R_{\kappa_2 L \kappa_1}^\pm = d_{\kappa_2 \kappa_1}^\pm \left\{ \begin{array}{l} -(E_1/|E_1|)[|E_1 - 1|(E_2 + 1)]^{1/2} \\ - [|E_1 + 1|(E_2 - 1)]^{1/2} \end{array} \right\} \sum_{n=0}^L \frac{(L+n)!}{n!(L-n)!} \left(\frac{1}{2k}\right)^n \frac{\Gamma(a)}{(k+p_1+p_2)^a} S_n^\pm, \quad (4.17)$$

where

$$d_{\kappa_2 \kappa_1}^\pm = \frac{(2p_2)^{\gamma_2 - 1/2} (2p_1)^{\gamma_1 - 1/2} e^{\pi(\gamma_2 + \gamma_1)/2} |\Gamma(\gamma_2 + i\gamma_2)| |\Gamma(\gamma_1 + i\gamma_1)|}{\Gamma(2\gamma_2 + 1) \Gamma(2\gamma_1 + 1)}$$

and

$$S_n^\pm = \text{Im} \left\{ e^{-i\pi(\gamma_1 + \gamma_2 - L - 1)/2} [K_1 K_2 \tilde{F}_2(b_1, b_2) \pm K_1 K_2^* \tilde{F}_2(b_1, b_2 - 1) \mp K_1^* K_2 \tilde{F}_2(b_1 - 1, b_2) - K_1^* K_2^* \tilde{F}_2(b_1 - 1, b_2 - 1)] \right\}.$$

In these formulas

$$\begin{aligned} a &= \gamma_1 + \gamma_2 - n, \\ b &= \gamma + 1 + i\gamma, \\ c &= 2\gamma + 1, \\ \gamma &= [\kappa^2 - (\alpha Z)^2]^{1/2}, \\ y &= \alpha Z E / p, \\ p &= (E^2 - 1)^{1/2}, \end{aligned} \quad (4.18)$$

and

$$K = (\gamma + i\gamma) e^{i\eta} = (\gamma + i\gamma) \frac{(\kappa - \gamma)p + i\alpha Z(E - 1)}{[2(E - 1)(E\kappa - \gamma)(\kappa - \gamma)]^{1/2}},$$

where we have suppressed the obvious indices 1 and 2, which refer to the initial- and final-state electrons in the matrix element (3.2), respectively. For pair production

$$\begin{aligned} \tilde{F}_2(b_1, b_2) &= F_2(a; b_1, b_2; c_1, c_2; x_1, x_2) \\ &= \sum_{i,j=0}^{\infty} \frac{(a)_{i+j} (b_1)_i (b_2)_j x_1^i x_2^j}{(c_1)_i (c_2)_j i! j!}, \end{aligned} \quad (4.19)$$

where

$$x_l = \frac{2p_l}{p_1 + p_2 + k}, \quad l = 1, 2$$

and

$$\begin{aligned} (a)_i &\equiv a(a+1)(a+2) \cdots (a+i-1) = \Gamma(a+i)/\Gamma(a), \\ (a)_0 &= 1. \end{aligned}$$

In the preceding equations k and E_2 denote the energies of the photon and the outgoing electron, respectively, while E_1 is the energy of the incoming negative-energy electron, which is to be substituted by

$$E_1 = -E_+, \quad (4.20)$$

where E_+ is the positron energy, according to

(3.4). For simplicity we omit this substitution in the formulas (4.17)–(4.19). It should be noticed that while $y_2 = \alpha Z E_2 / p_2$ is a positive quantity, y_1 is negative,³⁵

$$y_1 = -\alpha Z E_+ / p_+. \quad (4.21)$$

The numerical evaluation of the F_2 series is done most conveniently by writing the double series as a single series over ordinary hypergeometric series ${}_2F_1$,

$$\tilde{F}_2(b_1, b_2) = \sum_{i=0}^{\infty} \frac{(a)_i (b_1)_i x_1^i}{(c_1)_i i!} {}_2F_1(a+i, b_2; c_2; x_2).$$

Computing the first terms by means of the hypergeometric series, we may use a simple recurrence formula to calculate higher terms. A detailed description of the method of calculation may be found elsewhere.³⁶

We conclude the discussion of the radial integrals by noting that for bremsstrahlung we have the kinematic relation

$$k = E_1 - E_2 < p_1 - p_2,$$

so that for this case

$$\lim_{\epsilon \rightarrow 0} (|z_1| + |z_2|) = \frac{2(p_1 + p_2)}{k + p_1 + p_2} > 1.$$

Therefore the limit $\epsilon \rightarrow 0$ cannot be taken in (4.14); the F_2 function must be expressed in terms of another representation, i.e., an analytic continuation of (4.14), before the limit can be taken.³⁷

V. DIFFERENTIAL CROSS SECTIONS

With the matrix element \mathfrak{M}_P defined by (3.2) and (3.4) the differential cross section for pair production is given by

$$d\sigma_P = \frac{1}{(2\pi)^4} \frac{r_0^2}{\alpha} \frac{p_+ E_+ p_2 E_2}{k} dE_+ d\Omega_+ d\Omega_2 |\mathfrak{M}_P|^2, \quad (5.1)$$

where $\alpha = e^2/(\hbar c) \approx 137^{-1}$ is the fine-structure constant, $r_0 = e^2/(mc^2)$ is the "classical electron radius," k is the photon energy, and the in-

indices 2 and + refer to the final-state electron and positron, respectively. Using (3.5) and (3.8) we find

$$d^5\sigma_P(\vec{e}, \vec{\xi}_+, \vec{\xi}_-) = \frac{2r_0^2}{\alpha k^3} dE_+ d\Omega_+ d\Omega_2 \left| \sum_{\kappa_1 \kappa_2} \left(i^{l_1 - l_2} e^{i(\delta_2' + \delta_1')} \right) \times \sum_{M, \epsilon = \pm} [\chi_{\kappa_2 M + \epsilon/2}(\hat{p}_2) v(\vec{\xi}_2)]^* [\chi_{\kappa_1 M - \epsilon/2}(\hat{p}_1) v(\vec{\xi}_1)] e_{-\epsilon} A_{\kappa_2 \kappa_1 M}^\epsilon \right|^2, \quad (5.2)$$

where the index 1 refers to the initial-state negative-energy electron, which is equivalent to the positron, as discussed in Sec. III. This completely differential cross section depends on the photon polarization and on the spins and directions of both the final-state fermions. The symbols l_1 and δ_1' are shorthand for l_{κ_1} and δ_{κ_1}' , which are given by (2.6) and (2.13). The spin angular functions $\chi_{\kappa\mu}$ are given by (2.2), and the spin direction $\vec{\xi}_1$ and the unit vector \hat{p}_1 are related to the corresponding positron quantities by (3.4). The spinors $v(\vec{\xi})$ are defined by

$$\vec{\xi} = v^\dagger(\vec{\xi}) \vec{\sigma} v(\vec{\xi}),$$

and are given explicitly by the well-known formula

$$v(\vec{\xi}) = [2(1 + \xi_x)]^{-1/2} \begin{pmatrix} 1 + \xi_x \\ \xi_x + i\xi_y \end{pmatrix}. \quad (5.3)$$

The components e_\pm of the photon polarization are defined by (3.7), and the quantities $A_{\kappa_2 \kappa_1 M}^\epsilon$ are given by (3.9).

In order to be able to perform summation over polarization states and integration over angles analytically we write (5.2) in the form

$$d^5\sigma_P(\vec{e}, \vec{\xi}_+, \vec{\xi}_-) = \frac{2r_0^2}{\alpha k^3} dE_+ d\Omega_+ d\Omega_2 \sum_{\kappa_1 \bar{\kappa}_1 \kappa_2 \bar{\kappa}_2} \{ i^{\bar{l}_2 - l_2 + l_1 - \bar{l}_1} e^{i(\delta_2' + \delta_1' - \delta_2' - \delta_1')} \} \times \sum_{M \bar{M} \epsilon} [\chi_{\kappa_2 M + \epsilon/2}(\hat{p}_2) v(\vec{\xi}_2) v^\dagger(\vec{\xi}_2) \chi_{\kappa_2 M + \epsilon/2}(\hat{p}_2)] \times [\chi_{\kappa_1 M - \epsilon/2}(\hat{p}_1) v(\vec{\xi}_1) v^\dagger(\vec{\xi}_1) \chi_{\bar{\kappa}_1 M - \epsilon/2}(\hat{p}_1)] (e_{-\epsilon})^* e_{-\epsilon} (A_{\kappa_2 \bar{\kappa}_1 M}^\epsilon)^* A_{\kappa_2 \kappa_1 M}^\epsilon \}. \quad (5.4)$$

For the photon we may choose as orthogonal states right- and left-handed circular polarization (in the following denoted by RHC and LHC). Since we have chosen a coordinate system with $\hat{z} = \hat{k}$, the polarization vectors may be given by

$$\vec{e}_{\text{RHC, LHC}} = 2^{-1/2} \{1, \pm i, 0\}.$$

From (3.7) we then have

$$(e_{-\epsilon})_{\text{RHC, LHC}} = \delta_{\epsilon, \pm}.$$

Thus for an RHC photon only terms with $\bar{\epsilon} = \epsilon = +$ contribute in (5.4). For the projection operator vv^\dagger we use the relation

$$v(\vec{\xi}) v^\dagger(\vec{\xi}) = \frac{1}{2} (1 + \vec{\xi} \cdot \vec{\sigma}),$$

which makes the summation over spins trivial. After the spin of a particle has been summed over, the integration over its direction of motion is also trivial, since we may use the orthonormality relation

$$\int \chi_{\bar{\kappa} M + \epsilon/2}(\hat{p}) \chi_{\kappa M + \epsilon/2}(\hat{p}) d\Omega(\hat{p}) = \delta_{\bar{\kappa} \kappa} \delta_{M + \epsilon/2, M + \epsilon/2}. \quad (5.5)$$

As an example we give the pair-production cross section which is differential with respect to the electron angles; i.e., we have averaged (5.4) over the photon polarization, summed over the spins of the electron and the positron, and integrated over the positron angles:

$$d^3\sigma_P(\hat{p}_2, E_+) = \frac{2r_0^2}{\alpha k^3} dE_+ d\Omega_2 \times \sum_{\kappa_1 \bar{\kappa}_2 \bar{\kappa}_2} \left(i^{\bar{l}_2 - l_2} e^{i(\delta_2' - \delta_1')} \right) \times \sum_{M, \epsilon} [\chi_{\kappa_2 M + \epsilon/2}(\hat{p}_2) \chi_{\kappa_2 M + \epsilon/2}(\hat{p}_2)] \times (A_{\kappa_2 \kappa_1 M}^\epsilon)^* A_{\kappa_2 \kappa_1 M}^\epsilon \frac{1}{2}, \quad (5.6)$$

where the factor $\frac{1}{2}$ comes from the averaging over the photon polarization. In this formula $\epsilon = +$ and $\epsilon = -$ give the contributions from an RHC and an LHC photon, respectively. Since the cross section is differential only with respect to the momentum of one of the particles, and the spin of this particle has been summed over, one expects from symmetry that the contributions from the two pho-

ton states must be equal. This may also easily be verified explicitly.¹⁶ In (5.6) we may therefore remove the sum over ϵ and the factor $\frac{1}{2}$ and replace ϵ by plus or minus.

For the case that only the energy of one of the particles is observed, the cross section (5.6) may also be integrated over the direction of motion of the electron, and we get

$$\frac{d\sigma_P(E_+)}{dE_+} = \frac{2r_0^2}{\alpha k^3} \sum_{\kappa_1 \kappa_2 M} \left| A_{\kappa_2 \kappa_1 M}^+ \right|^2, \quad (5.7)$$

which is the positron energy spectrum. As men-

$$B_{\kappa_2 \kappa_1 M} = \sum_{L=L_{\min}}^{L_{\max}} (-)^{(L-L_{\min})/2} \left\{ \left[\frac{(\kappa_2 - M)(\kappa_1 - M)}{(2\kappa_2 + 1)(2\kappa_1 - 1)} \right]^{1/2} V(l_2 L l'_1 M) R_{\kappa_2 L \kappa_1}^+ \right. \\ \left. + \left[\frac{(\kappa_2 + M)(\kappa_1 + M)}{(2\kappa_2 - 1)(2\kappa_1 + 1)} \right]^{1/2} V(l'_2 L l_1 M) R_{\kappa_2 L \kappa_1}^- \right\}, \quad (5.9)$$

$$L_{\min} = \min(|l_2 - l'_1|, |l'_2 - l_1|), \quad L_{\max} = \max(l_2 + l'_1, l'_2 + l_1),$$

and l and l' are given in terms of κ by (2.6). The angular integrals V are given explicitly by (4.5), and the radial integrals R^\pm are given by (4.17)–(4.21). The sums over κ_1 and κ_2 in (5.8), in principle, run over all nonzero integers, while the limits on M are implicit in the angular integrals [cf. Eq. (4.4)]. It should be noticed that when r_0^2 is substituted by its numerical value ($\approx 7.94 \times 10^{-26}$ cm²), Eq. (5.8) gives the spectrum in, say cm²/($m_e c^2$), since we use the energy unit $m_e c^2 \approx 0.511$ MeV.

VI. NUMERICAL RESULTS

The main difficulty in the evaluation of numerical results lies in the calculation of the radial integrals, i.e., of the Appell functions. For photon energies close to the threshold the calculations are very easy, because the Appell series and the partial-wave sums both converge very fast. As the photon energy increases, the convergence becomes slower, so that the machine time required to calculate one point of the spectrum increases rather fast with the photon energy. For photon energies between 5 and 10 $m_e c^2$ we had to use a careful and rather complicated numerical procedure in order to obtain accurate results.³⁶

A. Positron Energy Spectrum

If we denote the positron energy spectrum (5.8) by

$$\frac{d\sigma}{dE_+}(E_p, E_e, Z),$$

where the first and the second arguments are the

tioned in Sec. III this formula might also have been derived by the direct use of spherical wave functions.¹⁶

From (4.2)–(4.4) it follows that the sum over L in (3.9) gives contributions only for even or only for odd L , depending on κ_1 and κ_2 . Therefore we may write

$$\frac{d\sigma_P(E_+)}{dE_+} = \frac{2r_0^2}{\alpha k^3} \sum_{\kappa_1 \kappa_2 M} (B_{\kappa_2 \kappa_1 M})^2, \quad (5.8)$$

where the real quantity B is given by

positron and electron energies, respectively, we have the following obvious relation:

$$\frac{d\sigma}{dE_+}(E_2, E_+, Z) = \frac{d\sigma}{dE_+}(E_+, E_2, -Z). \quad (6.1)$$

For the middle of the spectrum, where $E_+ = E_2 = \frac{1}{2}k$, Eq. (6.1) only shows that $d\sigma/dE_+$ at this point is an even function of Z . For $E_+ = \frac{1}{2}k$ we have, however, the relation¹⁶

$$[B_{\kappa_2 \kappa_1 M}(Z)]^2 = [B_{-\kappa_1 -\kappa_2 -M}(-Z)]^2, \quad (6.2)$$

where B is given by (5.9). The substitution $Z \rightarrow -Z$ only affects the radial integrals. By inspection of (4.17) and (4.18) we see that we only have to multiply the factor $d_{\kappa_2 \kappa_1}$ by $e^{-\pi(\nu_1 + \nu_2)}$, and change Z to $-Z$ in S_n^* . This is equivalent to complex conjugation of the Appell functions and the factors $K_1 K_2$, $K_1 K_2^*$, etc. Thus the relations (6.1) and (6.2) reduce the numerical work by a factor 2.

In Sec. I it was stated that the matrix element from which we calculate our cross sections corresponds to a simple vertex diagram in the Furry picture, with the radiation field included to first order and with exact Coulomb wave functions as fermion states. This vertex corresponds to an infinite sum of Feynman diagrams containing plane-wave states, where the interaction with the nuclear field is included to all orders, but with the radiation field to first order only. The lowest-order terms in this sum are the second-order diagrams corresponding to the Bethe-Heitler Born-approximation result. Therefore we may write for the positron spectrum

$$\frac{d\sigma}{dE_+}(E_+, E_2, Z) = \frac{d\sigma}{dE_+}(E_+, E_2)_B \left[1 + \sum_{i=1}^{\infty} c_i (\alpha Z)^i \right]. \quad (6.3)$$

where $d\sigma/dE_+(E_+, E_2)_B$ is the Bethe-Heitler spectrum³⁸ (which is proportional to Z^2). The coefficients c_i are functions of the energies,

$$c_i = c_i(E_+, E_2).$$

Equation (6.1) then requires

$$c_i(E_+, E_2) = -c_i(E_2, E_+), \quad i = 1, 3, 5, \dots \quad (6.4)$$

and

$$c_i(E_+, E_2) = c_i(E_2, E_+), \quad i = 2, 4, 6, \dots \quad (6.5)$$

Thus the contributions to the spectrum from the even (odd) powers of Z are symmetric (antisymmetric) under the interchange of the positron and electron energies.³⁹ It follows from (6.4) that

$$\begin{aligned} \frac{d\sigma}{dE_+}(\tfrac{1}{2}k, \tfrac{1}{2}k, Z) &= \frac{d\sigma}{dE_+}(\tfrac{1}{2}k, \tfrac{1}{2}k)_B \\ &\times \left[1 + \sum_{n=1}^{\infty} c_{2n}(\tfrac{1}{2}k, \tfrac{1}{2}k) (\alpha Z)^{2n} \right]. \end{aligned} \quad (6.6)$$

It also follows that the total cross section may be written

$$\sigma(k) = \sigma_B(k) \left[1 + \sum_{n=1}^{\infty} C_n(k) (\alpha Z)^{2n} \right], \quad (6.7)$$

where σ_B is the Bethe-Heitler total cross section, and

$$C_n(k) = \frac{1}{\sigma_B(k)} \int_1^{k-1} \frac{d\sigma}{dE_+}(E_+, E_2)_B c_{2n}(E_+, E_2) dE_+. \quad (6.8)$$

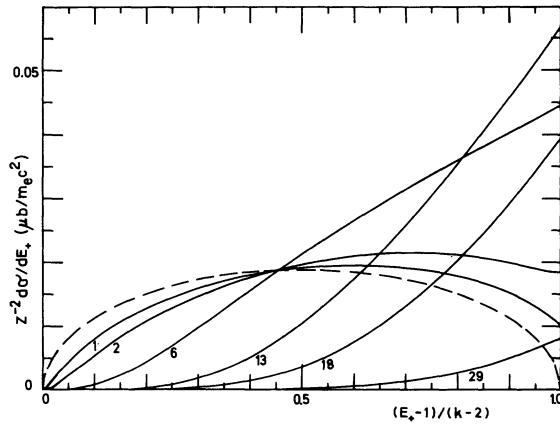


FIG. 1. Positron energy spectra for different atomic numbers Z (attached to the curves). The broken line gives the Bethe-Heitler spectrum. The photon energy (in units of $m_e c^2$) is $k = 2.01$.

Thus for the unscreened Coulomb potential the total pair-production cross section depends only on the photon energy and Z^2 .

We have calculated the spectrum for about 500 combinations of k and Z , mainly in order to be able to study the detailed behavior of the Coulomb correction to the total cross section. In Figs. 1-6 we give a selection of these spectra, illustrating the general behavior of $d\sigma/dE_+$ as a function of the energies and the atomic number.⁴⁰ These diagrams clearly show the importance of the Coulomb correction for the present range of photon energies. From the criteria of validity for the Born approximation,

$$\alpha Z E_+ / p_+ \ll 1 \quad \text{and} \quad \alpha Z E_2 / p_2 \ll 1,$$

it is expected that the Bethe-Heitler formula is insufficient for large Z , and even for small Z if we consider small values of the kinetic energy of one or both of the particles. This is confirmed by the behavior of the spectra in Figs. 1-6. Compared to the symmetrical Bethe-Heitler result the exact spectra are all seen to be asymmetrical. For small values of E_+ the Coulomb correction is negative; as E_+ increases, it changes sign. We notice that for small E_+ the spectrum behaves

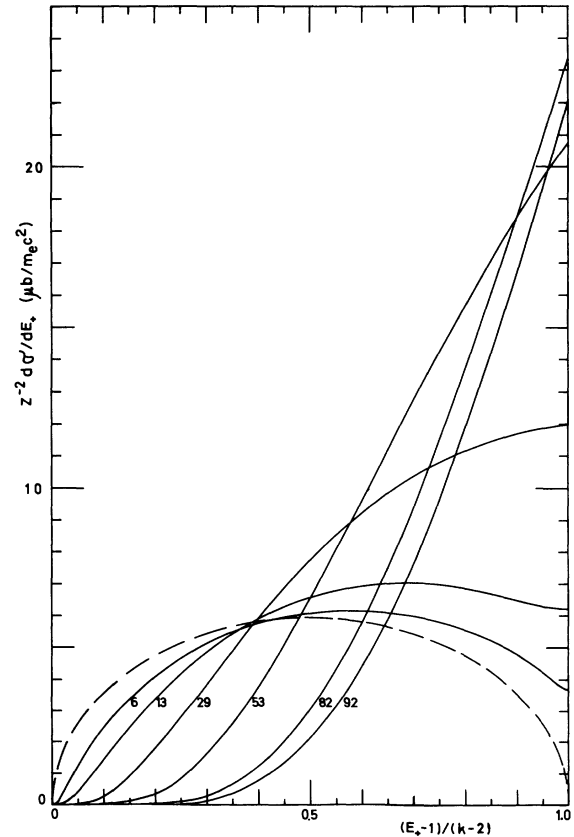
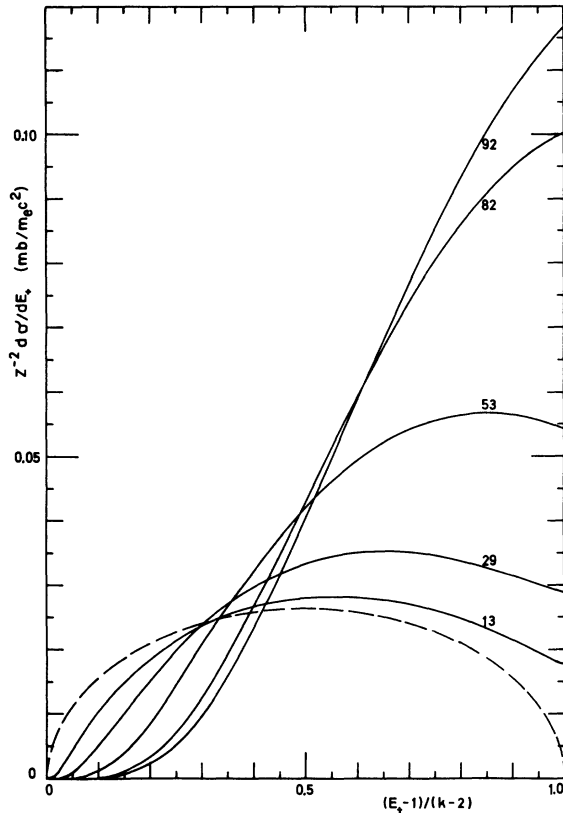
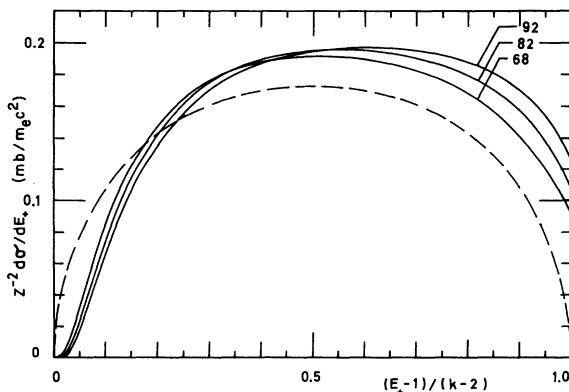
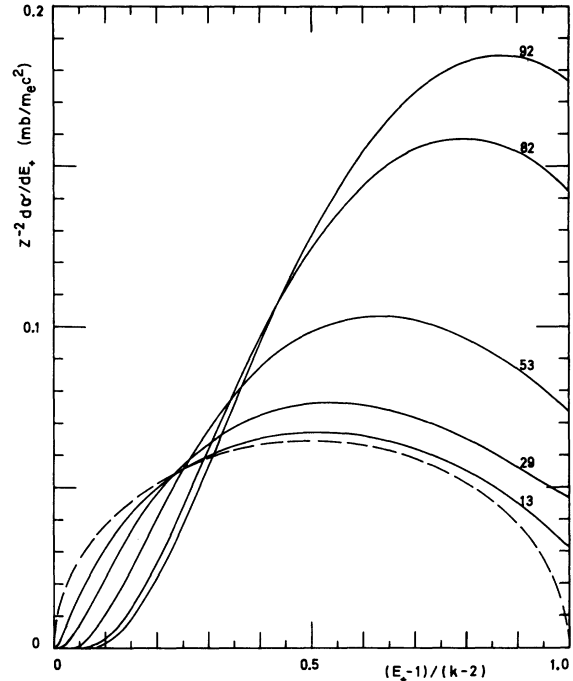


FIG. 2. Same as Fig. 1, for $k = 2.2$.

FIG. 3. Same as Fig. 1, for $k = 2.5$.

quite differently from the Born approximation, approaching zero when $p_+ \rightarrow 0$ in a manner similar to $e^{(-\text{const}/p_+)}$ (see what follows). At the right-hand side of the spectrum, where the electron energy $E_+ \rightarrow 1$, the exact cross section tends towards a finite value.

The Coulomb correction is seen to increase with Z , as expected. Thus for $Z = 92$ it is considerable even for $k = 10m_e c^2$, as seen in Fig. 6, although the correction to the total cross section nearly vanishes for this case (cf. Sec. VI B). As Z be-

FIG. 5. Same as Fig. 1, for $k = 7.0$.FIG. 4. Same as Fig. 1, for $k = 3.0$.

comes smaller it is seen that the range of validity of the Bethe-Heitler formula is extended towards smaller photon energies. Thus for $Z = 1$ the Born approximation is fairly good for photon energies down to about $2.10m_e c^2$ (see Fig. 1; and Fig. 1 of Ref. 17).

The reasons for the breakdown of the Born approximation for low energies are in a way two-fold: first, as the energies decrease, the wave functions close to the nucleus are more and more perturbed by the Coulomb field; second, the main contributions to the matrix element are known to come from a region limited roughly by $r \lesssim q_{\min}^{-1}$, where q_{\min} is the minimum recoil momentum of the nucleus, $q_{\min} = k - (k^2 - 4)^{1/2}$.

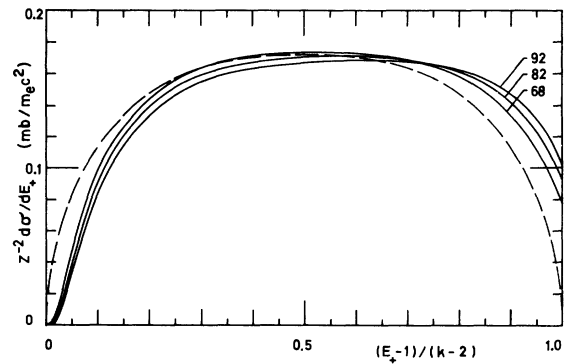
FIG. 6. Same as Fig. 1, for $k = 10.0$.

TABLE I. Total cross section σ obtained by the present theory and the Born-approximation total cross section σ_B , in b/atom. (The form 1.111-1 means 1.111×10^{-1} .)

$Z/k (m_e c^2)$	2.000 01	2.0001	2.0003	2.001	2.003	
1	6.271-21	2.092-16	5.725-15	1.796-13	4.378-12	
2	7.718-24	2.587-16	2.054-14	8.613-13	1.998-11	
4	3.252-31	1.391-17	1.610-14	2.776-12	9.419-11	
6			3.081-15	2.775-12	1.918-10	
13				1.179-13	1.568-10	
18				3.914-15		
29				6.631-19		
$Z^{-2}\sigma_B$	1.5095-19	1.5161-16	4.0936-15	1.5148-13	4.0788-12	
$Z/k (m_e c^2)$	2.01	2.02		2.03	2.04	
2	6.479-10	4.928-9				
4	2.985-9	2.158-8				
6	7.494-9	5.360-8		1.686-7	3.808-7	
13	2.873-8	2.853-7		9.600-7	2.193-6	
18	3.072-8	4.571-7		1.777-6	4.340-6	
24	2.063-8	5.257-7		2.538-6	6.957-6	
29	1.166-8	4.708-7		2.765-6	8.460-6	
37	3.495-9	3.001-7		2.439-6	8.998-6	
44	1.012-9	1.681-7		1.824-6	7.967-6	
53	1.737-10	6.752-8		1.065-6	5.788-6	
60		3.026-8		6.373-7	4.119-6	
68	7.154-12	1.123-8		3.298-7	2.594-6	
82	2.864-13			9.030-7	1.003-6	
92	2.671-14				4.652-7	
100	3.820-15					
$Z^{-2}\sigma_B$	1.4963-10	1.1808-9		3.9315-9	9.1942-9	
$Z/k (m_e c^2)$	2.05	2.07	2.10	2.12	2.15	2.20
6	7.168-7	1.859-6	5.086-6			3.475-5
13	4.110-6	1.044-5	2.768-5		8.283-5	1.784-4
18	8.419-6	2.200-5	5.878-5		1.742-4	3.708-4
24	1.445-5	4.065-5	1.135-4	1.878-4	3.425-4	7.275-4
29	1.885-5	5.756-5	1.705-4	2.875-4	5.333-4	1.144-3
32	2.081-5	6.710-5	2.070-4			
37	2.267-5	8.053-5	2.682-4	4.739-4	9.167-4	2.038-3
40	2.295-5	8.658-5	3.030-4			
44	2.248-5	9.209-5	3.453-4	6.390-4	1.297-3	3.016-3
53	1.893-5	9.366-5	4.134-4	8.172-4	1.778-3	4.437-3
60	1.512-5	8.692-5	4.350-4	9.115-4	2.102-3	5.574-3
68	1.089-5	7.437-5	4.324-4	9.653-4	2.384-3	6.801-3
74	8.160-6	6.341-5	4.127-4		2.521-3	7.612-3
82	5.310-6	4.913-5	3.719-4	9.315-4	2.602-3	8.486-3
92	2.914-6	3.346-5	3.062-4	8.333-4	2.547-3	9.161-3
100	1.719-6	2.347-5	2.501-4	7.276-4	2.390-3	9.306-3
$Z^{-2}\sigma_B$	1.7718-8	4.7340-8	1.3268-7	2.2340-7	4.1988-7	9.3469-7
$Z/k (m_e c^2)$	2.25	2.30	2.35	2.40	2.50	2.60
13	3.208-4	5.143-4	7.619-4	1.065-3	1.840-3	2.838-3
18	6.599-4	1.049-3	1.544-3	2.147-3	3.680-3	5.643-3
24	1.286-3	2.031-3	2.969-3	4.104-3	6.965-3	
29	2.025-3	3.191-3	4.650-3	6.403-3	1.079-2	1.632-2
37	3.661-3	5.799-3	8.455-3	1.163-2	1.947-2	

TABLE I (Continued)

$Z/k (m_e c^2)$	2.25	2.30	2.35	2.40	2.50	2.60
44	5.549-3	8.900-3	1.306-2	1.801-2	3.017-2	4.514-2
53	8.497-3	1.397-2	2.080-2	2.895-2	4.890-2	7.328-2
60	1.107-2	1.863-2	2.819-2	3.964-2	6.774-2	
68	1.414-2	2.452-2	3.786-2	5.403-2	9.400-2	1.428-1
74	1.640-2	2.913-2	4.577-2	6.613-2		
82	1.920-2	3.530-2	5.677-2	8.354-2	1.512-1	2.349-1
92	2.209-2	4.241-2	7.048-2	1.062-1	1.984-1	3.143-1
100	2.363-2	4.704-2	8.028-2	1.234-1	2.371-1	3.821-1
$Z^{-2}\sigma_B$	1.7171-6	2.7948-6	4.1861-6	5.9018-6	1.0321-5	1.6044-5

$Z/k (m_e c^2)$	2.80	3.00	3.25	3.50	3.75	4.25
13	5.455-3	8.805-3	1.383-2	1.956-2	2.583-2	
18	1.077-2	1.729-2	2.704-2	3.815-2	5.027-2	
29	3.053-2	4.836-2	7.475-2	1.045-1	1.368-1	2.059-1
44	8.257-2	1.283-1	1.944-1	2.677-1	3.459-1	5.106-1
53	1.333-1	2.053-1	3.076-1	4.195-1	5.375-1	7.826-1
68	2.611-1	3.995-1	5.905-1	7.935-1	1.003	1.425
82	4.376-1	6.710-1	9.856-1	1.311	1.638	2.277
92	5.971-1	9.209-1	1.351	1.788	2.218	3.041
100	7.391-1	1.148	1.686	2.224	2.747	3.727
$Z^{-2}\sigma_B$	3.1163-5	5.0612-5	7.9889-5	1.1345-4	1.5018-4	2.2982-4

$Z/k (m_e c^2)$	5.0	6.0	7.0	8.0	10.0
29	3.141-1				
53	1.153	1.629			
68	2.043	2.812	3.516	4.160	5.306
82	3.177	4.260	5.231	6.111	7.667
92	4.163	5.479	6.641	7.690	9.542
$Z^{-2}\sigma_B$	3.5656-4	5.2680-4	6.9102-4	8.4642-4	1.1296-3

Thus in the threshold limit the important contributions come from $r \lesssim O(\frac{1}{2})$. We get a more quantitative understanding of this by considering the nonrelativistic case. Then the relative densities of the electron and positron wave functions at the nucleus are⁴¹

$$\left| \frac{\Phi(r=0)}{\Phi(r=\infty)} \right|^2 = \frac{2\pi y_2}{1 - e^{-2\pi y_2}} \quad (6.9)$$

and

$$\left| \frac{\Phi^c(r=0)}{\Phi^c(r=\infty)} \right|^2 = \frac{2\pi y_4}{e^{2\pi y_4} - 1}, \quad (6.10)$$

where

$$y_2 = \alpha Z E_2 / p_2, \quad y_4 = \alpha Z E_4 / p_4.$$

Nishina, Tomonaga, and Sakata⁴² found that for nonrelativistic energies and small values of Z , the positron spectrum may be obtained from the Born

approximation by multiplication by the factors (6.9), (6.10), and another Coulomb correction factor $S(\alpha Z, k)$, which was given only to the order $(\alpha Z)^2$,⁴³

$$S(\alpha Z, k) = 1 + (\alpha Z)^2 \frac{3(\pi^2 + 8)}{64(k-2)} 2\pi. \quad (6.11)$$

With the expression

$$\left(\frac{d\sigma}{dE_+} \right)_{NR-B} = \alpha Z^2 r_0^2 \frac{k-2}{3} p_+ p_2 \quad (6.12)$$

for the nonrelativistic Born-approximation spectrum, the result of Nishina *et al.* then reads

$$\left(\frac{d\sigma}{dE_+} \right)_{NTS} = \left(\frac{d\sigma}{dE_+} \right)_{NR-B} \frac{2\pi y_4}{(e^{2\pi y_4} - 1)} \frac{2\pi y_2}{(1 - e^{-2\pi y_2})} S(\alpha Z, k), \quad (6.13)$$

valid for $k-2 \ll 1$ and $\alpha Z \ll 1$. The interesting thing here is that the form of the spectrum is given by the Born approximation (6.12) times the

factors (6.9) and (6.10). [This holds also for large Z , for which, however, the factor $S(\alpha Z, k)$ becomes too small, compared with the accurate results obtained from our exact formula.¹⁶] The behavior of our relativistic spectra for small E_+ is now explained by the factor (6.10), which makes the spectrum behave essentially like

$$e^{-2\pi\alpha Z/p_+} \quad (6.14)$$

for small p_+ . Thus the smallness of our exact values for $d\sigma/dE_+$ for small p_+ is due to the repulsion of the positron by the nucleus. At the other end of the spectrum, where $E_2 \rightarrow 1$, the factor (6.9) diverges as p_2^{-1} . This divergence is canceled by the phase-space factor p_2 in (6.12), giving a finite value of $d\sigma/dE_+$ in the limit $E_2 \rightarrow 1$.

The factor (6.14) gives a considerable reduction of $d\sigma/dE_+$ for the left-hand part of the spectrum. This part becomes larger, compared to the whole range $1 < E_+ < k-1$, when the photon energy decreases or when Z increases. As a result the ratio σ/σ_B between the exact and the Bethe-Heitler cross sections tends to zero in the limit $k \rightarrow 2$ (cf. Sec. VI B).

B. Total Cross Section

The total cross sections are obtained by numerical integration of the spectra,¹⁶

$$\sigma = \int_1^{k-1} \left(\frac{d\sigma}{dE_+} \right) dE_+. \quad (6.15)$$

In Table I we give σ in b/atom for a choice of photon energies between $2.00001 m_e c^2$ and $10 m_e c^2$. The accuracy of these results is of the order 0.1%.

We also include in the table the values of the Born-approximation total cross section σ_B . For most purposes σ_B may be obtained with sufficient accuracy from expansions given by Maximon.⁴⁴ These are given in the Appendix. As may be seen from formula (A1) in the Appendix and from the results given in Table I, the total cross section varies by several orders of magnitude in the energy region we are considering. It is therefore convenient to base the discussion of our exact results on the ratio σ/σ_B , which gives in addition a direct presentation of the Coulomb correction.

In Figs. 7-9 we give σ/σ_B as a function of the photon energy for various atomic numbers Z . It is seen from Fig. 7 that the Coulomb correction changes sign for photon energies around $10 m_e c^2$; the position of the crossing point depends on Z . As k decreases from this crossing-point value, the ratio σ/σ_B for a given Z increases toward a maximum, the position of which also depends on Z . For $Z=92$, for example, $(\sigma/\sigma_B)_{\max} \approx 2.31$ for $k \approx 2.62 m_e c^2$. When k is further decreased, σ/σ_B decreases rapidly and crosses unity again (see Fig. 8), and finally approaches zero at the threshold, as shown in Fig. 9. The behavior in the threshold region is due to the repulsion of the positron by the nucleus, which for small photon energies is accounted for by the factor (6.14), as discussed in Sec. VI A.

In order to display the Z dependence of the Coulomb correction we give in Figs. 10 and 11 the ratio σ/σ_B as a function of $(\alpha Z)^2$ for a selection of photon energies ranging between $2.03 m_e c^2$ and $10 m_e c^2$. From the curves we can draw some conclusions regarding the coefficients in the expan-

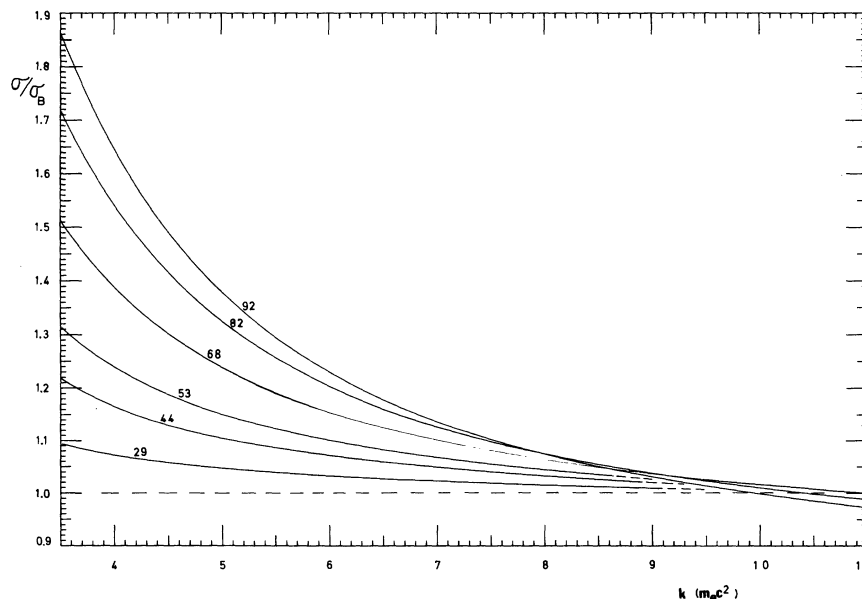


FIG. 7. Ratio between the exact and the Born-approximation total cross sections as a function of the photon energy k , for different atomic numbers (attached to the curves).

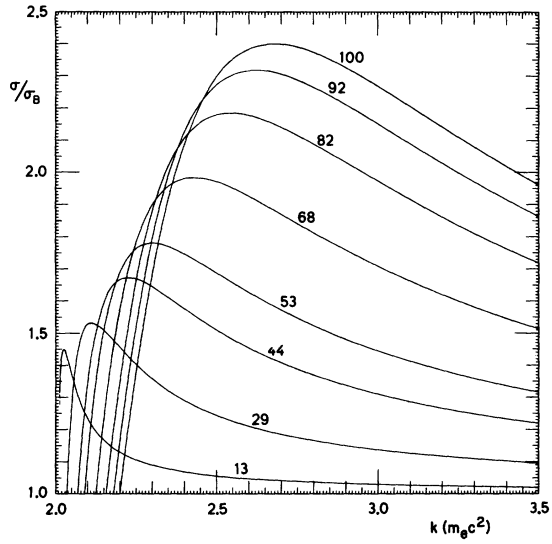


FIG. 8. Same as Fig. 7.

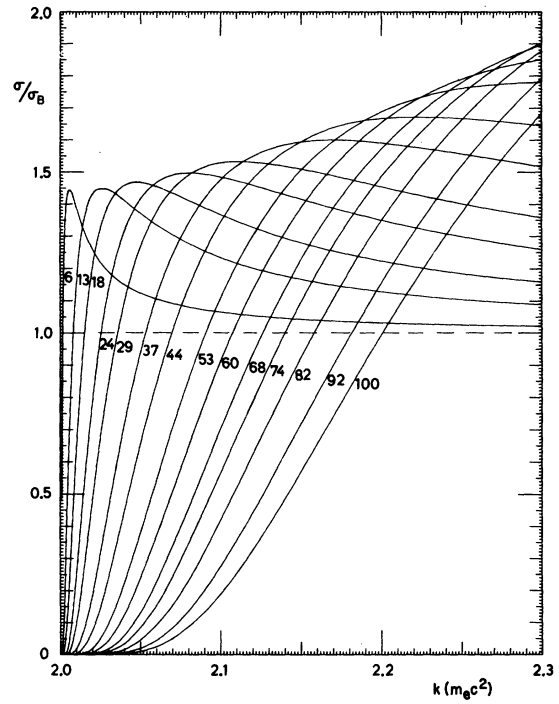


FIG. 9. Same as Fig. 7.

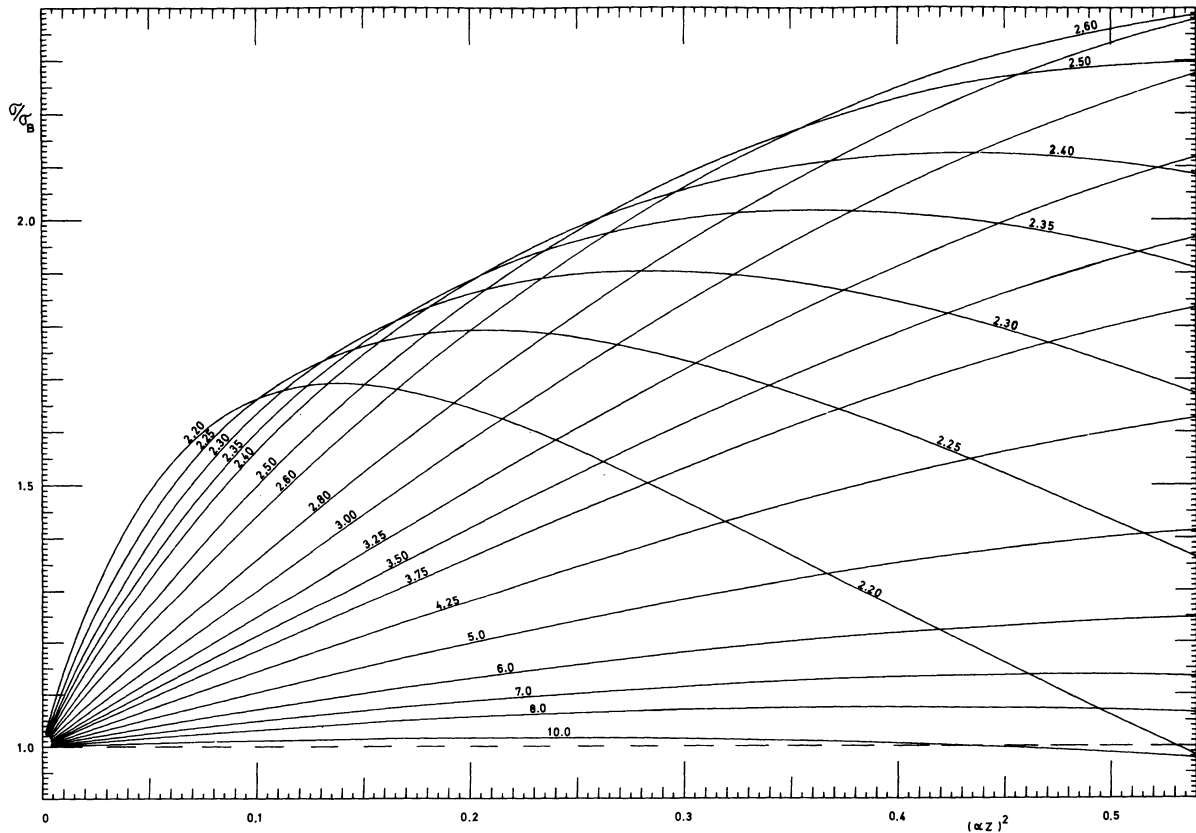


FIG. 10. Same ratio as in Fig. 7, but now as a function of $(\alpha Z)^2$, for different photon energies. The numbers attached to the curves give the photon energies in units of $m_e c^2$.

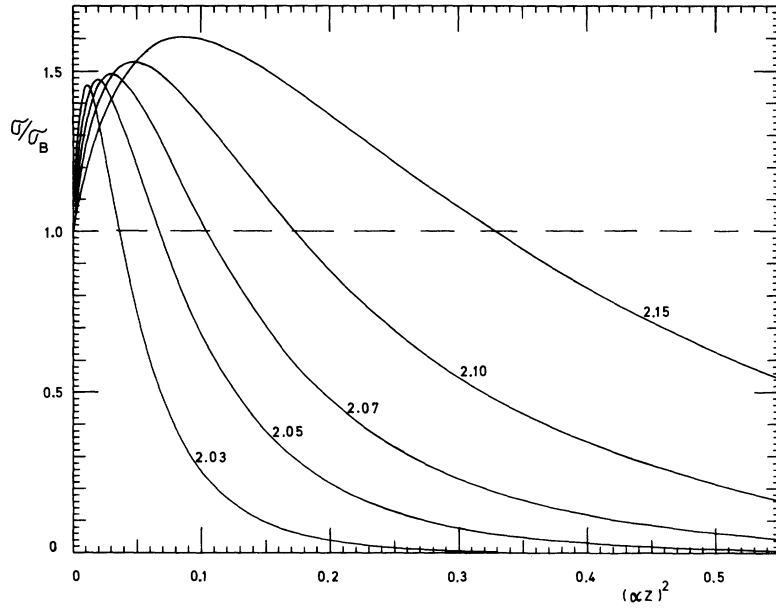


FIG. 11. Same as Fig. 10.

sion (6.7). It is seen that all the curves are approximately straight lines for small Z , as expected. For increasing Z all the curves are seen to fall below the straight-line extrapolation

$$\sigma/\sigma_B = 1 + C_1(k)(\alpha Z)^2.$$

For large photon energies the degree of this deviation is small, indicating that a few powers of $(\alpha Z)^2$ would suffice to describe the behavior, even for large Z . As k decreases it is obvious from Figs. 10 and 11 that the coefficients $C_i(k)$ become larger [for example, $C_1(k)$ is roughly proportional to $1/(k-2)$], and that an increasing number of terms in (6.7) contribute significantly. Thus, for $k \lesssim 2.20m_e c^2$ we see from Fig. 11 that σ/σ_B decreases nearly exponentially for large Z ,¹⁶ corresponding to an oscillatory behavior of the series (6.7), with large positive and negative terms which nearly cancel. For $k \lesssim 2.20m_e c^2$ the decrease of σ/σ_B with Z is so strong that even σ itself passes a maximum with respect to Z , in spite of the factor Z^2 in σ_B .¹⁶

VII. SUMMARY AND CONCLUSIONS

The results obtained in the present work give the Coulomb correction for photon energies between threshold and $10m_e c^2$, which is the region where the largest relative deviations between the exact and the Born-approximation cross sections occur. From the present results it is possible, e.g., by one- or two-way interpolation in Figs. 7-11, to find the ratio σ/σ_B with an accuracy of the order of 1% or better for any combination of k and Z in the region $k \lesssim 10m_e c^2$, $0 < Z \lesssim 100$. Nu-

merical values for the Born-approximation total cross section σ_B may easily be found from the expansions given by Maximon (see the Appendix).

Since the high-energy Coulomb correction obtained by Davies, Bethe, and Maximon³ is only valid for photon energies down to around $100m_e c^2$, there still remains an intermediate energy region, $10m_e c^2 < k \lesssim 100m_e c^2$, where the Coulomb correction to the total cross section is unknown theoretically. In order to see whether our results can be extrapolated into this energy region we have plotted σ/σ_B as a function of the ratio $1/(k-2)$, where k is the photon energy in units of $m_e c^2$.¹⁶ For $k \gtrsim 6m_e c^2$ the curves turn out to be very closely straight lines, so that we may write

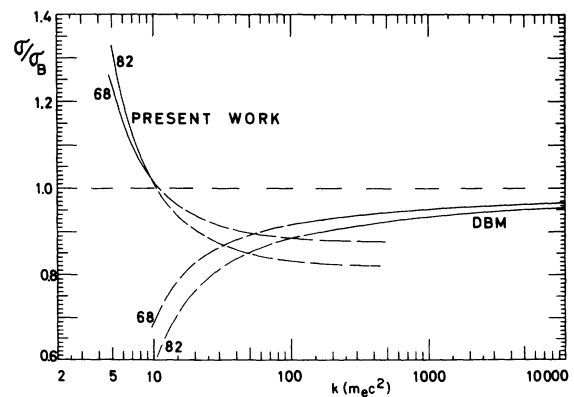


FIG. 12. Comparison between the ratio σ/σ_B obtained in the present work [extrapolated by means of Eq. (7.1)] and the corresponding ratio obtained from the Davies-Bethe-Maximon (DBM) unscreened total cross section, as functions of the photon energy k , for $Z = 68$ and $Z = 82$.

$$\sigma/\sigma_B = 1 + a + b/(k-2), \quad (7.1)$$

where a and b are functions of $(\alpha Z)^2$, which are found from our data to be well approximated by

$$a = -0.488(\alpha Z)^2 - 0.07(\alpha Z)^4,$$

$$b = 5.06(\alpha Z)^2 - 2.1(\alpha Z)^4.$$

The formula (7.1) fits our results for $6m_e c^2 \lesssim k < 10m_e c^2$ with errors of the order 0.1%. In view of the straight-line behavior of the curves (7.1),¹⁶ it seems reasonable to assume that (7.1) constitutes a good approximation also for photon energies a little larger than $10m_e c^2$, say up to $15m_e c^2$ or $20m_e c^2$. In Fig. 12 we have plotted (7.1) and the ratio $\sigma_{\text{DBM}}/\sigma_B$, where σ_{DBM} is the Davies-Bethe-Maximon unscreened total cross section, as functions of the photon energy k . The curves are seen to cross each other around $k = 50m_e c^2$, where both the results are probably incorrect. For $Z = 82$ the crossing point value is $\sigma/\sigma_B \approx 0.85$. It seems reasonable to assume that the true value of σ/σ_B is

$$\sigma_B = \alpha Z^2 r_0^2 \left\{ \frac{28}{9} \ln 2k - \frac{218}{27} + \left(\frac{2}{k} \right)^2 \left[6 \ln 2k - \frac{7}{2} + \frac{2}{3} \ln^3 2k - \ln^2 2k - \frac{\pi^2}{3} \ln 2k + \frac{\pi^2}{6} + 2\zeta(3) \right] - \left(\frac{2}{k} \right)^4 \left[\frac{3}{16} \ln 2k + \frac{1}{8} \right] - \left(\frac{2}{k} \right)^8 \left[\frac{29}{9 \times 256} \ln 2k - \frac{77}{27 \times 512} \right] + O \left[\left(\frac{2}{k} \right)^8 \right] \right\}, \quad (A2)$$

with

$$\zeta(3) = \sum_{n=1}^{\infty} \frac{1}{n^3} = 1.202\,056\,9\dots$$

If (A1) is used for $k \lesssim 3.8m_e c^2$ and (A2) is used for

above 0.85 so that the curves (7.1) and the DBM curves will be joined in a smooth manner.¹⁷ This question can, however, only be settled by further theoretical calculations or by accurate experiments.

APPENDIX

The unscreened Born-approximation total cross section for pair production may be found from the following expansions given by Maximon⁴⁴: The first expansion,

$$\sigma_B = \alpha Z^2 r_0^2 \frac{2\pi}{3} \left(\frac{k-2}{k} \right)^3 \times \left[1 + \frac{1}{2}\epsilon + \frac{23}{40}\epsilon^2 + \frac{11}{60}\epsilon^3 + \frac{23}{960}\epsilon^4 + O(\epsilon^5) \right], \quad (A1)$$

with

$$\epsilon = \frac{2k-4}{2+k+2(2k)^{1/2}},$$

converges rapidly in the threshold region, while the second expansion is best suited for high energies,

$k \gtrsim 3.8m_e c^2$, comparison with the results obtained by accurate numerical integration of the Bethe-Heitler formula³⁸ shows that the relative error is always less than 10^{-4} .

*Present address: Nordita, Copenhagen, Denmark.

¹J. C. Jaeger and H. R. Hulme, Proc. R. Soc. (London) A148, 708 (1935). Similar calculations on the photoelectric effect were made by H. R. Hulme, J. McDougall, R. A. Buckingham, and R. H. Fowler, Proc. R. Soc. (London) A149, 131 (1935).

²J. C. Jaeger and H. R. Hulme, Proc. R. Soc. (London) A153, 443 (1936); J. C. Jaeger, Nature (Lond.) 137, 781 (1936); and Nature (Lond.) 148, 86 (1941).

³H. Davies, H. A. Bethe, and L. C. Maximon, Phys. Rev. 93, 788 (1954).

⁴H. A. Olsen, Springer Tracts Mod. Phys. 44, 102 (1968).

⁵S. Hultberg, B. Nagel, and P. Olsson, Ark. Fys. 20, 555 (1962); Ark. Fys. 38, 1 (1968).

⁶H. Rozics and W. R. Johnson, Phys. Rev. 135, B56 (1964).

⁷W. R. Alling and W. R. Johnson, Phys. Rev. 139, A1050 (1965).

⁸J. J. Matese and W. R. Johnson, Phys. Rev. 140, A1 (1965).

⁹R. H. Pratt, R. D. Levee, R. L. Pexton, and W. Aron, Phys. Rev. 134, A898 (1964).

¹⁰H. Hall and E. C. Sullivan, Phys. Rev. 152, 4 (1966).

¹¹G. Rakavy and A. Ron, Phys. Rev. 159, 50 (1967).

¹²R. D. Schmickley and R. H. Pratt, Phys. Rev. 164, 104 (1967).

¹³H. Brysk and C. D. Zerby, Phys. Rev. 171, 292 (1968).

¹⁴H. Brysk, C. D. Zerby, and S. K. Penny, Phys. Rev. 180, 104 (1969).

¹⁵H. K. Tseng and R. H. Pratt, Phys. Rev. A 1, 528 (1970); Phys. Rev. A 3, 100 (1971) (bremsstrahlung); and Phys. Rev. A 4, 1835 (1971) (pair production).

¹⁶A more detailed discussion can be found in I. Øverbø, Arkiv for Det Fysiske Seminar i Trondheim, No. 9, 1970 (unpublished).

¹⁷A brief report on some of the results has been published before by I. Øverbø, K. J. Mork, and H. A. Olsen, Phys. Rev. 175, 1978 (1968).

¹⁸K. Mork and H. Olsen, Phys. Rev. 140, B1661 (1965); Phys. Rev. 166, 1862 (1968).

¹⁹Reference 4, p. 190.

²⁰We use the same conventions for the spherical harmonics and the Clebsch-Gordan coefficients as, e.g., E. U. Condon and G. H. Shortley, *The Theory of Atomic Spectra* (Cambridge U. P., Cambridge, England, 1964).

²¹C. G. Darwin, Proc. R. Soc. (Lond.) A118, 654 (1928).

- ²²W. Gordon, *Z. Phys.* **48**, 11 (1928).
²³N. F. Mott, *Proc. R. Soc. (London)* **A124**, 425 (1929).
²⁴M. E. Rose, *Phys. Rev.* **51**, 484 (1937).
²⁵M. E. Rose, *Relativistic Electron Theory* (Wiley, New York, 1961).
²⁶P. O. M. Olsson, *Ark. Fys.* **15**, 131 (1959).
²⁷M. Kolsrud, *Phys. Norv.* **2**, 43 (1966).
²⁸See, for example, Ref. 4, pp. 85–92.
²⁹W. Gordon, *Z. Phys.* **48**, 180 (1928).
³⁰It is also possible to write formula (2.20) in a form involving only the κ sum, the sum over μ and the Clebsch-Gordan coefficients being absent. For a discussion of this formula see Ref. 4, p. 100.
³¹G. Racah, *Phys. Rev.* **62**, 438 (1942).
³²*Bateman Manuscript Project, Higher Transcendental Functions*, edited by A. Erdélyi (McGraw-Hill, New York, 1953), Vol. I.
³³P. Appell and J. Kampé de Fériet, *Fonctions Hypergéométriques et Hypersphériques—Polynômes d'Hermite* (Gauthier-Villars, Paris, 1926).
³⁴H. Jeffreys and B. S. Jeffreys, *Methods of Mathematical Physics* (Cambridge U. P., Cambridge, England, 1946), pp. 39–40.
³⁵Note that y_1 was given with the wrong sign in Ref. 17. The numerical calculations reported in this paper were, however, based on the correct formula, as given here by Eq. (4.21).
³⁶For details regarding the numerical procedure, see Ref. 16, Appendix E.
³⁷We are going to publish a work on bremsstrahlung where such a method is used. For an account of the method of analytic continuation, see Ref. 16, or I. Øverbø and K. J. Mork, report of work prior to publication, University of Trondheim, 1971.
³⁸W. Heitler, *The Quantum Theory of Radiation*, 3rd ed., (Oxford U. P., London, England, 1954), p. 258.
³⁹Numerical values for some of the coefficients c_i are given for a few combinations of k and E_+ in Ref. 16, p. 159.
⁴⁰Spectra for $k = 2.1m_e c^2$ and $k = 5m_e c^2$ are given in Ref. 17. Additional diagrams may be found in Ref. 16.
⁴¹Reference 25, p. 196.
⁴²Y. Nishina, S. Tomonaga, and S. Sakata, *Sci. Pap. Inst. Phys. Chem. Res. Suppl. Tokyo* **24**, 17 (1934).
⁴³The factor 2π in the last term of (6.11) was not present in the formula given by Nishina, Tomonaga, and Sakata. However, comparison with our exact results indicates that a factor of this order should be present. It is our conjecture that it is a constant factor of 2π (cf. Ref. 16).
⁴⁴L. C. Maximon, *J. Res. Natl. Bur. Stand. (U.S.)* **B 72**, 79 (1968).

Atomic Quadrupole Moments of the Excited States of the Rare Gases. II*

R. M. Sternheimer

Brookhaven National Laboratory, Upton, New York 11973

(Received 28 February 1973)

In a recent paper, the atomic quadrupole shielding factor R_Θ has been calculated for the excited states $np^3n's$ ($n' = n + 1$) of the rare gases, in connection with an experiment of Sandars and Stewart. The previous calculations included only the first-order term $R_{\Theta,1}$ in the perturbation $v_1'(n's - d)$ of the excited $n's$ electron. The values of $R_{\Theta,1}$ were found to be in good agreement with experiment. In the present paper, the terms of second order in v_1' have been evaluated. Their inclusion improves appreciably the agreement of $R_{\Theta,calc}$ with the experimental values of Sandars and Stewart, in particular for the cases of Kr and Xe.

I. INTRODUCTION

In a recent paper¹ we have carried out detailed calculations of the atomic quadrupole moments of the rare gases in the excited states $np^5n's$ ($n' = n + 1$), where $n = 2$ for Ne, $n = 3$ for Ar, $n = 4$ for Kr, and $n = 5$ for Xe. These calculations were performed in connection with an experiment of Sandars and Stewart,² in which it was found that the atomic quadrupole moments Θ_{atom} are always much smaller in magnitude than the values expected from the np vacancy alone $[\Theta(np)]$, and in fact for Kr and Xe have opposite sign to $\Theta(np)$. The theoretical value of $\Theta(np)$, in the notation of Buckingham,³ is $-0.2e\langle r^2 \rangle_{np}$, where $\langle r^2 \rangle_{np}$ is the expectation value of r^2 for the np -vacancy wave function. It was suggested by Sandars⁴ that the disagreement between the observed Θ_{atom} and the

calculated $\Theta(np)$ is probably due to the $n's - d$ distortion of the $n's$ electron charge distribution arising from the quadrupole potential produced by the np vacancy. If this induced quadrupole moment is denoted by $\Theta(n's - d)$, one can define a shielding factor R_Θ by the equation

$$R_\Theta = -\Theta(n's - d)/\Theta(np), \quad (1)$$

so that the total Θ for the atom can be written as follows:

$$\Theta_{atom} = \Theta(np) + \Theta(n's - d) = \Theta(np)(1 - R_\Theta). \quad (2)$$

Sandars and Stewart² have expressed their observed results for Θ_{atom} in terms of an experimental shielding factor $R_{\Theta,expt}$ for each of the four rare gases.

In the previous paper (Ref. 1), we have calculated the theoretical values of R_Θ , using the same np